

1 Structure optimization for improving the strength and ductility of 2 heterogeneous carbon nanotube/Al-Cu-Mg composites

3 K. Ma^{1,2,3}, Z.Y. Liu^{1,*}, K. Liu³, X. Grant Chen³, B.L. Xiao^{1,**}, Z.Y. Ma¹

4 ¹Shi-changxu Innovation Center for Advanced Materials, Institute of Metal Research, Chinese
5 Academy of Science, Shenyang, 110016, China

6 ²School of Materials Science and Engineering, University of Science and Technology of
7 China, Shenyang, 110016, China

8 ³Department of Applied Science, University of Québec at Chicoutimi, Saguenay, Québec
9 G7H 2B1, Canada

10 Abstract:

11 Heterogeneous carbon nanotube (CNT)/Al-Cu-Mg composites, consisting of ductile
12 zones (DZs) free of CNTs and brittle zones (BZs) rich of CNTs, were fabricated in powder
13 metallurgy route. It was shown that the grain size and width of the DZs in the heterogeneous
14 composites could be controlled by high energy ball milling (HEBM) on additional Al-Cu-Mg
15 alloy powders. Appropriate grain refinement in the DZs and a medium DZ width were
16 identified to be beneficial for improving the strength-ductility. Under the optimized condition,
17 a heterogeneous CNT/Al-Cu-Mg composite exhibited 88% increase in the elongation and 2%
18 increase in the tensile strength compared to the uniform composite. Although the yield
19 strength of the heterogeneous composite was lower than that of the uniform composite, the
20 appropriate grain refinement in the DZs was good for alleviating the low yield phenomenon.
21 Furthermore, the abundant grain boundaries could reduce the local slip bands passing through
22 the DZs, which could significantly relax the stress concentration of the BZs. As a result, the
23 medium width DZs could contribute more to the plastic deformation, thereby further
24 improving the strength-ductility. Finally, a model was proposed to assist the design of the

*Corresponding authors. E-mail address: zyliu@imr.ac.cn (Z.Y. Liu).

**Corresponding author. E-mail address: blxiao@imr.ac.cn (B.L. Xiao).

1 heterogeneous structure parameters. The calculated optimized DZ size was in accordance with
2 the DZ width of the heterogeneous composite with the best strength-ductility.

3 **Keywords:** Carbon Nanotube, Al matrix composite, Heterogeneous, Mechanical property

4 **1. Introduction**

5 Carbon nanotubes (CNTs), as a typical kind of nanoscale materials, have extremely high
6 strength (about 30 GPa) and elastic modulus (about 1 TPa) [1, 2]. Therefore, they are
7 considered as ideal reinforcements for metals. In the past decade, many studies have shown
8 that the strength and modulus of CNT/Metal composites could be enhanced compared with
9 those of the matrixes [3-10]. The major strengthening mechanisms of CNT/Metal composites
10 are the load transfer from the matrix to CNTs and the grain refinement caused by CNT
11 addition [11-19]. Since the grain size of CNT/Metal composites is very small, the dislocation
12 storage ability is weakened and the elongation (EI) is very low, limiting their engineering
13 application in wider fields.

14 The design of heterogeneous structures consisting of ductile zones (DZs) and brittle
15 zones (BZs) through inhomogeneous distribution of reinforcements or grain sizes, was
16 demonstrated to be a potentially effective way to overcome the strength-ductility trade off of
17 ultrafine grained (UFG) metals or composites [4, 20-26]. In our previous investigation [19],
18 we fabricated a heterogeneous CNT/Al-Cu-Mg composite by powder metallurgy (PM)
19 method combined with subsequent hot extrusion, and achieved more than twice EI with nearly
20 no loss of the ultimate tensile strength (UTS) compared to the uniform CNT/Al-Cu-Mg
21 composite.

22 Although the strength-ductility of heterogeneous CNT/Al composite was improved, the
23 new drawback of low yield strength (YS) was introduced [28]. Since the relatively low
24 strength of the DZs, preferential plastic deformation of the DZs would occur at the early stage
25 of tension, resulting in the phenomenon of low-stress yielding first in the DZs and then

1 overall yielding in whole zones [27]. The low YS of heterogeneous materials had also been
2 confirmed by other scholars in the laminate Ti-Al composites and bimodal 5083Al
3 composites [28-29]. The low YS of the heterogeneous materials is not conducive to the
4 engineering application, so it is necessary to further optimize the heterogeneous structure to
5 overcome this drawback.

6 It should be mentioned that Salama et al. [26] have fabricated a series heterogeneous
7 CNT/Al composites, and found that the composites with DZs originated from milled Al
8 powders had higher strength. In general, milling could result in grain refinement for ductile
9 metal powders. Therefore, their investigation indicates that the grain refinement might be an
10 effect strategy for alleviating the low stress yielding in heterogeneous composites. However,
11 too serious grain refinement has the risk of reducing the ductility of the DZs due to the
12 strength-ductility trade-off. Proper grain refinement could be an effective way to improve the
13 strength and maintain high ductility of the DZs. For example, Hayes *et al.* [30] reported that
14 Al-3wt.% Mg alloy with grain size around 500 nm had the best combination of strength and
15 ductility.

16 Furthermore, in order to maximize the potential of the heterogeneous structures, many
17 investigators focused on the optimization of the heterogeneous structure parameters, through
18 the optimum dimension of the DZs [31-35]. However, nearly no investigations have been
19 conducted on the grain size within the DZs of the heterogeneous materials. Lu *et al.* [36]
20 found that the grain size transition mode of the DZs and BZs significantly affected the
21 strength-ductility, and the gradient transition from nano to micron grains was better than that
22 sudden transition from nano to micron. However, it is still unclear whether this was suitable
23 for the DZ and BZ grain design in the heterogeneous CNT/Al composites.

24 In this study, the heterogeneous CNT/Al composites consisting of DZs free of CNTs and
25 ultrafine grained BZs rich of CNTs, were fabricated in high energy ball milling (HEBM) and

1 powder metallurgy (PM) route. Both the effects of DZ width and grain size within the DZs on
2 the mechanical properties were studied. The aim is to (a) alleviate the low YS of CNT/Al
3 composites induced by the heterogeneous structure, (b) optimize heterogeneous structure
4 parameters to achieve higher strength-ductility, and (c) propose a model to guide the design of
5 the heterogeneous structures.

6 **2. Experimental**

7 In this study, CNT/2009Al composites with different heterogeneous structures were
8 fabricated through HEBM and PM routes as shown in Fig. 1. Atomized 2009Al (Al-4wt.%
9 Cu-1.5wt.% Mg) powders with approximately 10 μm diameters were used as the raw
10 materials. CNTs (~98% purity) fabricated by chemical vapor deposition had an outer diameter
11 of 10-20 nm and a length of ~5 μm . 2.25 and 3 vol.% CNTs without extra pre-treatment were
12 ball milled with the as-received 2009Al powders at a rotation rate of 250 rpm with a ball to
13 powder ratio of 15:1 for 10 h using an attritor. Meanwhile, the 2009Al powders were
14 respectively ball milled for different times (0 h, 3 h, 4 h and 5 h). 25% of these above 2009Al
15 powders milled for different times were then respectively mixed with 75% as-milled 3 vol.%
16 CNT/2009Al composite powders using a dual axis mixer at a rotation rate of 50 rpm for 6 h.

17 The mixed composite powders containing 75% as-milled 3 vol.% CNT/2009Al
18 composite powders and 25% 2009Al powders milled for different times, were cold compacted
19 and vacuum hot pressed into billets under a pressure of 50 MPa at 813 K. Then the billets
20 were extruded into bars at 743 K with an extrusion ratio of 16:1. The extruded bars were
21 solution treated at 773 K for 2 h, quenched into water and naturally aged for 4 days (T4 state).
22 Finally, four heterogeneous composites were fabricated. For convenience, the heterogeneous
23 composites obtained by mixing the as-milled 3 vol.% CNT/2009Al composite powders and
24 2009Al powders milled for X hours were abbreviated as 3% CNT-X h DZ. For comparison,
25 the as-milled 2.25 and 3 vol.% CNT/2009Al composite powders, the as-received 2009Al

1 powders and 2009Al powders milled for 4 h were fabricated into the composites and
2 unreinforced alloy using the same hot-densification and heat treatment processes as those of
3 the heterogeneous composites, and the corresponding materials were respectively labelled as
4 uniform 2.25 vol.% CNT/2009Al, uniform 3 vol.% CNT/2009Al, 2009Al-0 h and 2009Al-4 h,
5 respectively.

6 Optical microscopy (OM, Zeiss Axiovert 200MAT) was used to examine DZ
7 morphology and distribution, and the samples used for OM observation were polished without
8 etching. Substructure sizes of the milled 2009Al powders were analyzed using X-ray
9 diffraction (XRD, D8 Advance) with a Cu K α radiation source through the Scherrer formula
10 [37]. The powder morphologies and the fracture surfaces of the tensile specimens were
11 observed using a field emission scanning electron microscope (FESEM, SUPRA 55). The
12 grain structure, CNT distribution and dislocation state were observed by transmission electron
13 microscopy (TEM, Tecnai G2 20). TEM specimens were cut by electrical discharge
14 machining, ground to a thickness of 60 μm , punched to disks with a diameter of 3 mm, then
15 dimpled to a minimum thickness of 20 μm and finally ion-beam thinned by a Gatan Model
16 691 ion milling system. Tensile specimens with a gauge diameter of 5 mm and a length of 30
17 mm were machined from the extruded bars with the axis parallel to the extrusion direction.
18 Tensile tests were carried out at a strain rate of 10^{-3} s^{-1} using an Instron 8862 tester. An
19 Instron static axial clip-on extensometer with a gauge length of 25 mm was used to measure
20 the El.

21 Finite element method (FEM) models were built to investigate the effect of the DZs with
22 different parameters on the stress and strain distributions. Three different DZ bands, namely
23 the narrow DZ with low strength (Narrow DZ-LS), narrow DZ with high strength (Narrow
24 DZ-HS) and medium DZ with high strength (Medium DZ-HS) were respectively embedded in
25 the BZs. The YS of low strength and high strength DZ bands were 300 MPa and 500 MPa,

1 respectively. Tensile loading to 720 MPa stress was applied on these models. The linear work
2 hardening equation was used to model the plastic properties of the DZs and BZs, which
3 follows $\sigma = \sigma_y + M\varepsilon_p$ (where σ_y is the YS, M is the strength coefficient, and ε_p is the
4 plastic strain).

5 **3. Results**

6 **3.1 Morphology evolutions of 2009Al powders during milling**

7 Fig. 2 shows the morphologies of 2009Al powders milled for different times. It can be
8 seen that the powders underwent the typical milling powder evolution. At the early stage of
9 ball milling time of 3 h, the 2009Al powders changed from spherical (Fig. 2a) to flaky
10 morphology (Fig. 2b), which was in accordance with the flattening mechanism. As the milling
11 time increased from 3 to 4 h, the radius of flake Al powders decreased while the thickness
12 increased (Fig. 2(c)(d)), indicating the appearance of cold-welding. After 4 h milling, both the
13 radius and thickness increased with increasing the time (Fig. 2(e)(f)), which demonstrates that
14 the cold-welding dominated at this stage.

15 As the result of the severe plastic deformation during milling, the grain or sub-grain size
16 of the milled metals would be seriously refined, due to the dislocation cutting mechanism [3,
17 38]. The XRD patterns of the 2009Al powders milled for different times are shown in Fig.
18 2(g). It can be seen the half-height width of the diffraction peak increased continuously with
19 increasing the milling time, which means that the sub-grain size was significantly decreased.
20 The calculated sub-grain sizes of the milled 2009Al powders according to Scherrer formula
21 [37] are shown in Fig. 2(h). It demonstrates that the sub-grain size of the milled 2009Al
22 powders was even refined to <100 nm and gradually decreased with increasing the milling
23 time. These above results indicate that the morphology dimension and grain size of the
24 2009Al powders could be well controlled by adjusting the milling time.

25 **3.2 Microstructure of heterogeneous CNT/2009Al composites**

1 Fig. 3 shows the OM images of different heterogeneous CNT/2009Al composites.
2 According to our previous investigations [12, 39, 40], the dark regions were the BZs rich of
3 CNTs which formed by the milled 3 vol.% CNT/2009Al powders, while the white zones were
4 the DZs free of CNTs which originated from the addition of milled 2009Al powders. It can be
5 found that all the DZs were elongated along the extrusion direction, and the addition of
6 2009Al powders under different milling times (Fig. 2) led to quite different DZ morphologies.
7 The measured structure parameters of the DZs are listed in Table. 1. It can be seen that the DZ
8 width was in accordance with the addition of the milled 2009Al powders. That is, the milled
9 powders with larger dimension after cold welding led to the larger DZ width (Fig. 3). Further,
10 the DZ contents of all heterogeneous composites were almost the same, which were much
11 close to the quantity of additional milled 2009Al powders.

12 Fig. 4 shows the typical TEM images of the DZs for different heterogeneous composites.
13 It can be seen that the grain morphologies of the DZs in these composites were quite different.
14 For 3% CNT-0 h DZ, the grains within the DZs were elongated with a width of $\sim 1.5 \mu\text{m}$ and a
15 much larger length of $\sim 5 \mu\text{m}$ (Fig. 4(a)). The large ratio of length to width of the grains could
16 be attributed to the plastic deformation and dynamic recovery of the additional as-received
17 2009Al powders during hot extrusion. For 3% CNT-3 h DZ, the grains in the DZs still
18 retained the elongated morphology, however, both the width ($\sim 600 \text{ nm}$) and length ($\sim 1.5 \mu\text{m}$)
19 of the grains within the DZs (Fig. 4(b)) were smaller than those of 3% CNT-0 h DZ. For 3%
20 CNT-4 h DZ, the width ($\sim 500 \text{ nm}$) and length ($\sim 1 \mu\text{m}$) of the elongated grains in the DZs
21 further decreased, and some grains changed to equiaxed shape (Fig. 4(c)). For 3% CNT-5 h
22 DZ, the grains within the DZs were nearly equiaxed (Fig. 4(d)), with the average grain size of
23 about 500 nm.

24 It can be concluded that the grain size within the DZs decreased with extending the
25 milling time on the addition 2009Al powders. On the whole, the grain morphology evolution

1 within the DZs was consistent with the sub-grain size evolution of the addition 2009Al
2 powders characterized by XRD (Fig. 2(h)), which was the result of severe plastic deformation
3 of Al powders during milling. It should be mentioned that the grain size of the DZs in
4 heterogeneous composites was much larger than that evaluated by XRD, which was believed
5 to result from the grain coarsening during hot densification process.

6 Fig. 5 shows the typical TEM images of the BZs in the 3% CNT-4 h DZ. It can be seen
7 that the grain size within the BZs was in the UFG range of 100 to 300 nm (Fig. 5(a)), which
8 was much smaller than that in the DZs. The magnified image demonstrates that CNTs with
9 average length of ~100 nm (marked by black arrows) were uniformly distributed in the BZs
10 with UFG (Fig. 5(b)). The much finer grains within the BZs could be attributed to the longer
11 milling time of the 3 vol.% CNT/2009Al powders and the inhibition of CNTs on the grain
12 growth [9, 39]. High resolution TEM image indicates that the interface between CNT and Al
13 matrix was well bonded, and the structure integrity of CNTs maintained well (Fig. 5(c)).

14 **3.3 Mechanical properties**

15 Tensile stress-strain curves for the uniform 2.25 vol.% CNT/2009Al and heterogeneous
16 3% CNT-X h DZ composites are shown in Fig. 6(a). The uniform 2.25 vol.% CNT/2009Al
17 composite had a high YS of 671 MPa and high UTS of 707 MPa, but the El was as low as
18 2.5%. Compared with the uniform 2.25 vol.% CNT/2009Al composite, the heterogeneous 3%
19 CNT-X h DZ composites had the same total CNT content of 2.25 vol.% but exhibited a much
20 higher El, which demonstrates a positive toughening effect of the heterogeneous structure.
21 Furthermore, it should be noted that all the curve slopes of the heterogeneous composites
22 dropped as the stress increased higher than about 450 MPa (marked by black arrow). This first
23 low yielding phenomenon could be attributed to the local plastic deformation of the
24 low-strength DZs. With further increasing the stress, the whole zone of the composite yielded
25 and formed the global yielding. YS_I and YS_{II} were used to define the local and the global YS,

1 respectively.

2 Fig. 6(b) shows the tensile properties for different heterogeneous composites, and all the
3 property values are in detail listed in Table 2. It can be found that the YS_I and YS_{II} gradually
4 increased with increasing the milling time on the addition 2009Al powders, while the UTS as
5 well as El first increased and then decreased. The highest UTS of 720 MPa and El of 4.7%
6 were achieved for the 3% CNT-4 h DZ. For the optimized heterogeneous composite, the UTS
7 was even higher than that of the uniform composites and the El was nearly twice that of the
8 uniform composites. It was also reported by Salama et al [26] that the strength and El of the
9 heterogeneous CNT/Al composite increased simultaneously, as the DZ materials underwent
10 proper milling. This phenomenon could be related to the morphology and grain structure
11 change of DZs. The effect of DZ structure parameters on the property evolution will be
12 discussed in Section 4.2.

13 Fig. 7 shows the fractographs of the 3% CNT-0 h DZ and 3% CNT-4 h DZ. For the 3%
14 CNT-0 h DZ, dense and fine dimples with sizes smaller than 1 μm could be observed (Fig.
15 7(a)). It is believed that the fine dimples were the result of BZ fracture. The magnified
16 fractograph in Fig. 7(b) exhibits many ridge-shaped zones with a dimension of about 2 μm
17 dispersed in the fine dimples. No CNTs could be found within the ridge-shaped zones, and the
18 dimension of the ridge-shaped zones was close to the width of the DZs (Table 1). All of these
19 indicate that the ridge-shaped zones originated from the DZ fracture. Further, micro-pores
20 (marked by red circles) were found at the boundaries between the DZs and the BZs, which
21 could be caused by the large stress concentration at these positions [27]. For 3% CNT-4 h DZ,
22 the dimples were larger than those for 3% CNT-0 h DZ (Fig. 7(c)), indicating more plastic
23 deformation before fracture. No large ridge-shaped zones or micro pores could be observed
24 on the magnified fractograph (Fig. 7(d)), which might be related to the small stress
25 concentration between the DZs and the BZs resulting from the small grain size difference.

1 4. Discussion

2 4.1 Alleviation of low yield strength in heterogeneous composites

3 It was reported that the preferential deformation of the DZs could lead to a YS drop [28,
4 29]. In the present study, the double yielding occurring in the heterogeneous composites also
5 confirmed this point. As the applied stress on the DZs exceeded their YS, local plastic
6 deformation of the DZs occurred. Because the YS of the BZs was much higher than that of
7 the DZs, the BZs were at the stage of elastic deformation until the applied stress was higher
8 than the YS of the BZs. The early yielding was caused by the local plastic deformation of low
9 strength DZs, and its value was lower than the YS of the BZs.

10 The heterogeneous composite can be regarded as a BZ material (CNT/2009Al)
11 reinforced DZ material (2009Al). The rule-of-mixtures was used to calculate the tensile
12 strength of the heterogeneous composites based on the BZs and DZs [40-43]:

$$13 \sigma_H = \sigma_{BZ} V_{BZ} + \sigma_{DZ} V_{DZ} \quad (1)$$

14 where V_{BZ} and V_{DZ} are the volume fractions of the BZs and DZs, respectively; σ_H , σ_{BZ}
15 and σ_{DZ} are the strengths of the heterogeneous composite, BZs and DZs, respectively. For 3%
16 CNT-0 h DZ and 3% CNT-4 h DZ, their V_{BZ} and V_{DZ} values were 0.75 and 0.25,
17 respectively. As shown in Table 2, it is known that the YS of the DZs in 3% CNT-0 h DZ
18 (2009Al-0 h), the DZs in 3% CNT-4 h DZ (2009Al-4 h), and the BZs in these two
19 heterogeneous composites (uniform 3 vol.% CNT/2009Al) were 305, 515 and 672 MPa,
20 respectively.

21 According to the rule-of-mixtures, the calculated YS of 3% CNT-0 h DZ and 3% CNT-4
22 h DZ were 580 MPa and 633 MPa, respectively. It can be found that the YS_I of 3% CNT-0 h
23 DZ (574 MPa) and 3% CNT-4 h DZ (620 MPa) were higher than the YS of the DZs, but
24 slightly lower than the YS calculated by the rule-of-mixtures, and the YS_{II} of 3% CNT-0 h
25 DZ (625 MPa) and 3% CNT-4 h DZ (655 MPa) were higher than the YS calculated by the

1 rule-of-mixtures. This could be related to the different stress distributions between the BZs
2 and DZs.

3 Because the BZs contained abundant CNTs, its modulus was much higher than that of
4 the DZs [15, 44, 45]. Under the same elastic strain, the applied stress on the BZs was higher
5 than that on the DZs. Therefore, as the stress applied on the DZs reached their YS, the stress
6 applied on the BZs would be higher than that on the DZs, resulting in the YS_I being higher
7 than the YS of the DZs. However, because the stress applied on the BZs had not yet reached
8 the YS of the BZs, the YS_I would be lower than the YS calculated by the rule-of-mixtures. As
9 the loading increased, when the applied stress on the BZs just reached their YS, the DZs had
10 already in the plastic deformation stage, and thus the stress applied on the DZs exceeded the
11 YS of the DZs. Therefore, the YS_{II} would be higher than that of the YS calculated by the
12 rule-of-mixtures.

13 According to the rule-of-mixtures, increasing the strength of the DZs or BZs could lead
14 to the strength improvement of the whole heterogeneous composites. This is in consistent
15 with the results in Fig. 6(b): the grain size in the DZs decreased with increasing the milling
16 time of additional 2009Al powders, thereby increasing the YS of the DZs according to the
17 Hall-Petch relationship [46]:

$$18 \quad \sigma_y = \sigma_0 + kd^{-1/2} \quad (2)$$

19 where σ_y is the YS, σ_0 and k are constants, d is the average grain size. Because there
20 was no change in the BZs, σ_{BZ} was constant, the YS increase of the DZ would lead to the
21 YS_I and YS_{II} increase of the heterogeneous composites.

22 **4.2 Ductility improvement of heterogeneous composites**

23 Many studies showed that the plastic deformation of the DZs could contribute to the El
24 improvement of heterogeneous materials [40, 47-51]. Witkin *et al.* [48] investigated the
25 mechanical properties of heterogeneous Al-Mg alloys with different DZ contents, and found

1 that the more DZs led to the higher El. This was mainly because the DZs had higher
2 dislocation storage capability, and a large number of DZs could promote more space for
3 dislocation storage. In this study, although the DZ contents with different heterogeneous
4 composites were the same, the El were quite different. This could be related to different
5 morphology dimensions and grain sizes in the DZs.

6 Fig. 8 shows the microstructures of two typical heterogeneous composites after 2%
7 plastic strain. For 3% CNT-0 h DZ (Fig. 8(a)), it can be seen that large numbers of
8 dislocations were intertwined and arranged into narrow band structure, indicating the
9 formation of local slip bands in the DZs. As a typical microstructure in the coarse grains, local
10 slip bands would promote the local deformation and decrease the dislocation storage
11 capability [52, 53]. For 3% CNT-4 h DZ (Fig. 8(b)), the grain size within the DZs was smaller
12 and no local slip bands were found. Instead, many dislocations were uniformly distributed in
13 the DZs. The absence of local slip band could be due to the various grain orientations and
14 abundant grain boundaries within the DZs, thereby inhibiting the long-range directional
15 slipping of dislocations. Because no local slip bands formed in 3% CNT-4 h DZ, the
16 deformation in the DZs would be more uniform and dislocation storage capability would be
17 higher, which was good for improving the ductility.

18 The effect of heterogeneous structure evolutions on the mechanical properties can be
19 further investigated by 2-D FEM models, as shown in Fig. 9. Three heterogeneous composites
20 containing different DZ structures including Narrow DZ-LS (Fig. 9(a)), Narrow DZ-HS (Fig.
21 9(b)) and Medium DZ-HS (Fig. 9(c)) were established, in which the LS and HS were used to
22 simulate the effect of large grains and small grains in the DZs, respectively. Under external
23 loading, the maximum stress in the BZ of the composite containing Narrow DZ-LS (Fig. 9(d))
24 was higher than that of the other two composites (Fig. 9(e) and (f)). This was because the low
25 strength of the DZs bore very low applied loading and required the BZs to bear higher applied

1 loading. The maximum internal stresses of the three composites were as follows: Narrow
2 DZ-LS with 895 MPa, Narrow DZ-HS with 812 MPa, and Medium DZ-HS with 853 MPa.
3 High stress concentration in the composite containing Narrow DZ-LS could cause the
4 premature failure and lead to a low El.

5 From the strain distribution maps (Fig. 9(g), (h) and (i)), it can be found that the DZs
6 bore higher strain. The preferential deformation in the DZs with high ductility helped to
7 increase the El. However, a careful comparison of the three materials shows that the strain
8 contributions of the DZs were quite different. The composite containing Narrow DZ-HS (Fig.
9 9(h)) had a smaller strain in the DZs than the other two composites (Fig. 9(g) and (i)), which
10 means that the DZs did not contribute much to the El. This could be responsible for its lower
11 El than the composite containing Medium DZ-HS.

12 Finally, the effect of DZ structures on the El can be concluded. For the composite
13 containing the DZs with narrow width and the large grain size (3% CNT-0 h DZ), local slip
14 bands within the DZs were easy to form, and the stress concentration at the boundaries
15 between the DZs and the BZs was large, which would deteriorate the ductility. For the
16 composite containing the DZs with narrow width and fine grain size (3% CNT-3 h DZ), the
17 stress concentration at the boundaries between the DZs and BZs was small. However, because
18 the width of the DZs was very small, the deformation of the DZs would be limited by the
19 neighboring BZs, resulting in a low contribution of the DZs to the ductility, and its El was
20 even lower than that of 3% CNT-0 h DZ. For the composite containing the DZs with medium
21 width and fine grain size (3% CNT-4 h DZ), the abundant grain boundaries within the DZs
22 could hinder the formation of local slip bands, the stress concentration at the boundaries
23 between the DZs and the BZs was weakened. Further, because the width of the DZs was
24 relatively large, the adjacent BZs had less restraint on the deformation of the DZs. As a result,
25 the DZs could contribute sufficient plastic deformation, thereby contributing to a higher El.

1 For the composite containing the DZs with large width and fine grain size (3% CNT-5 h DZ),
2 the distance between the adjacent DZs was too far, DZs could not passivate the cracks in time
3 when micro cracks were formed in the BZs, so the EI would decrease.

4 **4.3. Design of DZ structures in heterogeneous materials**

5 From the previous investigations [27, 34, 40] and the present experimental results, it can
6 be seen that the strength-ductility was indeed improved due to the heterogeneous structures.
7 However, due to the different DZ structure parameters, such as the content, width, and grain
8 size of the DZ, the toughening effects were quite different. In order to fully exploit the
9 property potential of the heterogeneous structures, coupling optimization of the DZ structure
10 parameters was necessary.

11 According to the theory of linear-elastic fracture mechanics, as a micro-crack appears in
12 the material, the plastic deformation near the tip of the micro-crack can be induced to blunt
13 the micro-crack, thereby inhibiting the further propagation of the micro-crack and preventing
14 catastrophic fracture. For the heterogeneous materials, cracks are easily to form in the BZs
15 due to their poor ductility. As the micro-crack propagates to the DZs, plastic deformation of
16 the DZs is induced, and then cracks can be effectively blunted, as shown in Fig. 10(a).

17 The remaining toughness (ΔK) of the materials containing micro-crack is affected by
18 two aspects. On one hand, the remaining toughness is decreased due to the formation of
19 cracks. The stress intensity factor at the crack tip can be used to quantify the toughness loss
20 [54]:

$$21 \quad K_{loss} = Y_I \sigma \sqrt{a} \quad (3)$$

22 where K_{loss} is the toughness loss caused by the crack formation, Y_I is the constant, σ is the
23 applied stress and a is the half length of the crack. On the other hand, the plastic deformation
24 formed in the DZs can relax the local stress at the crack tip, resulting in an increase in the
25 toughness. According to the elastic-plastic theory, the maximum tolerable strength intensity

1 factor under the plane strain state is [54]:

$$2 \quad K_{plastic} = \sqrt{4\sqrt{2}\pi R_0 \sigma_y^{DZ}} \leq K_{IC}^{DZ} \quad (4)$$

3 where $K_{plastic}$ is the toughness increase caused by the plastic deformation, R_0 is the size of
 4 the plastic deformation zone (Plastic-Zone), σ_y^{DZ} is the YS of the DZs, K_{IC}^{DZ} is the fracture
 5 toughness of the DZs. $K_{plastic}$ cannot be infinitely increased, and its maximum $K_{plastic}$ ($K_{p,max}$)
 6 is equal to K_{IC}^{DZ} . Finally, the remaining toughness of the heterogeneous materials can be
 7 expressed as:

$$8 \quad \Delta K = K_{plastic} - K_{loss} = \sqrt{4\sqrt{2}\pi R_0 \sigma_y^{DZ}} - Y_{II} \sigma \sqrt{a} \quad (5)$$

9 The DZ size is defined as R . When R is very small, the size of the plastic zone will be
 10 limited by the geometric size of the DZs. Under this condition, $R_0 = R$. When R is large
 11 enough, R_0 is determined by $K_{p,max}$, and cannot be further affected by R . Define $R_{critical}$ as
 12 the maximum R_0 , and it can be calculated from Eq. (4):

$$13 \quad R_{critical} = \frac{1}{4\sqrt{2}\pi} \left(\frac{K_{p,max}}{\sigma_y} \right)^2 \quad (6)$$

14 Because the width of the crack is determined by the distance between the DZs, the width
 15 of the crack will also be enlarged or reduced with changing the size of the DZs. Then, Eq. (5)
 16 can be expressed as:

$$17 \quad \begin{cases} \Delta K = M_0 \sqrt{R}, & (R \leq R_{critical}) \\ \Delta K = K_{p,max} - Y_{II} \sigma \sqrt{R}, & (R > R_{critical}) \end{cases} \quad (7)$$

18 where M_0 and Y_{II} are constants. From Eq. (7), it can be found as $R = R_{critical}$, ΔK reaches the
 19 maximum, so the best size of the DZs can be determined, which is equal to $R_{critical}$. However,
 20 since there are many DZs distributed in the heterogeneous materials, the crack propagation
 21 will be affected by the joint action of multiple neighboring DZs (Fig. 10(b)). Because the

1 toughness of the BZs (K_{IC}^{BZ}) is very small, $K_{p,max}$ can be regarded as approximately equal to
 2 $V_{DZ}K_{IC}^{DZ}$, which is related to the volume fraction of the DZs (V_{DZ}), and considering the
 3 contribution of YS of BZs (σ_y^{BZ}) to the plastic zone, Eq. (7) can be changed to:

$$4 \quad K_{plastic} = \sqrt{4\sqrt{2}\pi R_0} \left[\sigma_y^{DZ} V_{DZ} + \sigma_y^{BZ} (1 - V_{DZ}) \right] \leq V_{DZ} K_{IC}^{DZ} + (1 - V_{DZ}) K_{IC}^{BZ} \approx V_{DZ} K_{IC}^{DZ} \quad (8)$$

5 The best DZ size can be calculated:

$$6 \quad R_{critical} = \frac{1}{4\sqrt{2}\pi} \left(\frac{V_{DZ} K_{IC}^{DZ}}{\sigma_y^{DZ} V_{DZ} + \sigma_y^{BZ} (1 - V_{DZ})} \right)^2 \quad (9)$$

7 From Eq. (9), it can be found that with the increase of YS of the DZs, the best DZ size
 8 will be decreased. Substitute the V_{DZ} with 25%, σ_y^{DZ} with 515 MPa (the YS of 2009Al-4h),
 9 σ_y^{BZ} with 672 MPa (the YS of uniform 3 vol.% CNT/2009Al) and K_{IC}^{DZ} of 29 MPa \sqrt{m} [55]
 10 into Eq. (9), the best DZ size is determined to 7.39 μm . It needs to be noted that the calculated
 11 best DZ size is very similar to the DZ width of 3% CNT-4 h DZ (6.62 μm), which proves the
 12 validity of Eq. (9).

13 5. Conclusions

14 (1) CNT/2009Al composites with a heterogeneous structure consisting of CNT-free DZs and
 15 CNT-rich BZs were successfully fabricated using HEBM combined with powder
 16 metallurgy. CNTs with good structure integrity were dispersed in the BZs with grain
 17 sizes of about 200 nm, while the DZs were aligned along the extruding direction with
 18 grain sizes no smaller than 500 nm.

19 (2) The DZ structures were controlled by HEBM processing to the alloy powders. With
 20 increasing the HEBM time from 0 to 5 h, the DZ width decreased first and then increased,
 21 while the grain sizes within the DZs decreased continuously. The heterogeneous
 22 composites containing the DZs with smaller grain size had the higher YS.

- 1 (3) 3% CNT-4 h DZ had the UTS of 720 MPa and El of 4.7%, both of them were higher than
2 those of the uniform composites and other heterogeneous composites. The grain size of
3 about 500 nm in the DZs of 3% CNT-4 h DZ relaxed the stress concentration at the
4 boundaries between the DZs and BZs, while the medium width of DZs provided enough
5 space for the preferential deformation of the DZs to enhance ductility.
- 6 (4) A model based on crack blunting was proposed for assisting the heterogeneous structure
7 design. The calculated best DZ size was very close to the DZ width of the heterogeneous
8 composite with the best ductility.

9 **Acknowledge**

10 This work was financially supported by the Key Research Program of Frontier Sciences,
11 CAS (No. QYZDJ-SSW-JSC015), the National Natural Science Foundation of China (Nos.
12 51931009, 51871214 and 51871215), the National Key R&D Program of China (No.
13 2017YFB0703104) and the Youth Innovation Promotion Association CAS (No. 2020197). K.
14 Ma would like to acknowledge the support from China Scholarship Council.

15 **References**

- 16 [1] T.I.Y.A. Sumio Iijima, Helical microtubules of graphitic carbon, *Nature* 354(6348) (1991)
17 56-58.
- 18 [2] M. Trojanowicz, Analytical applications of carbon nanotubes: a review, *TrAC Trends in*
19 *Analytical Chemistry* 25(5) (2006) 480-489.
- 20 [3] Z.Y. Liu, B.L. Xiao, W.G. Wang, Z.Y. Ma, Modelling of carbon nanotube dispersion and
21 strengthening mechanisms in Al matrix composites prepared by high energy ball
22 milling-powder metallurgy method, *Composites Part A* 94 (2017) 189-198.
- 23 [4] H. Wei, Z. Li, D.-B. Xiong, Z. Tan, G. Fan, Z. Qin, D. Zhang, Towards strong and stiff
24 carbon nanotube-reinforced high-strength aluminum alloy composites through a
25 microlaminated architecture design, *Scripta Mater.* 75(Supplement C) (2014) 30-33.

- 1 [5] Z.Y. Liu, S.J. Xu, B.L. Xiao, P. Xue, W.G. Wang, Z.Y. Ma, Effect of ball-milling time on
2 mechanical properties of carbon nanotubes reinforced aluminum matrix composites,
3 Composites Part A 43(12) (2012) 2161-2168.
- 4 [6] H. Ghobadi, A. Nemati, T. Ebadzadeh, Z. Sadeghian, H. Barzegar-Bafrooei, Improving
5 CNT distribution and mechanical properties of MWCNT reinforced alumina matrix, Mater. Sci.
6 Eng., A 617 (2014) 110-114.
- 7 [7] X. Yang, T. Zou, C. Shi, E. Liu, C. He, N. Zhao, Effect of carbon nanotube (CNT) content
8 on the properties of in-situ synthesis CNT reinforced Al composites, Mater. Sci. Eng., A 660
9 (2016) 11-18.
- 10 [8] S. Bi, B.L. Xiao, Z.H. Ji, B.S. Liu, Z.Y. Liu, Z.Y. Ma, Dispersion and Damage of Carbon
11 Nanotubes in Carbon Nanotube/7055Al Composites During High-Energy Ball Milling Process,
12 Acta Metallurgica Sinica (English Letters) (2020).
13 <https://doi.org/10.1007/s40195-020-01138-5>.
- 14 [9] K. Ma, Z. Liu, X. Zhang, B. Xiao, Z. Ma, Fabrication of high strength carbon
15 nanotube/7055Al composite by powder metallurgy combined with subsequent hot extrusion,
16 SCIENCE CHINA Technological Sciences (2020). <https://doi.org/10.1007/s11431-020-17158>.
- 17 [10] F. Mokdad, D.L. Chen, Z.Y. Liu, D.R. Ni, B.L. Xiao, Z.Y. Ma, Hot deformation and
18 activation energy of a CNT-reinforced aluminum matrix nanocomposite, Mater. Sci. Eng., A
19 695 (2017) 322-331.
- 20 [11] F. Mokdad, D.L. Chen, Z.Y. Liu, D.R. Ni, B.L. Xiao, Z.Y. Ma, Three-dimensional
21 processing maps and microstructural evolution of a CNT-reinforced Al-Cu-Mg nanocomposite,
22 Mater. Sci. Eng., A 702 (2017) 425-437.
- 23 [12] K. Ma, Z.Y. Liu, X.X. Zhang, B.L. Xiao, Z.Y. Ma, Hot deformation behavior and
24 microstructure evolution of carbon nanotube/7055Al composite, J. Alloys Compd. 854 (2021)
25 157275.

- 1 [13] S. Bi, Z.Y. Liu, B.H. Yu, G.N. Ma, L.H. Wu, B.L. Xiao, Z.Y. Ma, Superplastic
2 deformation behavior of carbon nanotube reinforced 7055 Al alloy composites, *Mater. Sci.*
3 *Eng., A* 797 (2020) 140263.
- 4 [14] R. Xu, Z. Tan, G. Fan, G. Ji, Z. Li, Q. Guo, Z. Li, D. Zhang, Microstructure-based
5 modeling on structure-mechanical property relationships in carbon nanotube/aluminum
6 composites, *Int. J. Plast.* 120 (2019) 278-295.
- 7 [15] B.K. Choi, G.H. Yoon, S. Lee, Molecular dynamics studies of CNT-reinforced aluminum
8 composites under uniaxial tensile loading, *Composites Part B: Engineering* 91 (2016) 119-125.
- 9 [16] J.G. Park, D.H. Keum, Y.H. Lee, Strengthening mechanisms in carbon
10 nanotube-reinforced aluminum composites, *Carbon* 95 (2015) 690-698.
- 11 [17] Z.Y. Liu, B.L. Xiao, W.G. Wang, Z.Y. Ma, Singly dispersed carbon nanotube/aluminum
12 composites fabricated by powder metallurgy combined with friction stir processing, *Carbon*
13 50(5) (2012) 1843-1852.
- 14 [18] Z.Y. Liu, B.L. Xiao, W.G. Wang, Z.Y. Ma, Developing high-performance aluminum
15 matrix composites with directionally aligned carbon nanotubes by combining friction stir
16 processing and subsequent rolling, *Carbon* 62 (2013) 35-42.
- 17 [19] Z.Y. Liu, B.L. Xiao, W.G. Wang, Z.Y. Ma, Analysis of carbon nanotube shortening and
18 composite strengthening in carbon nanotube/aluminum composites fabricated by multi-pass
19 friction stir processing, *Carbon* 69 (2014) 264-274.
- 20 [20] L. Jiang, H. Yang, J.K. Yee, X. Mo, T. Topping, E.J. Lavernia, J.M. Schoenung,
21 Toughening of aluminum matrix nanocomposites via spatial arrays of boron carbide spherical
22 nanoparticles, *Acta Mater.* 103 (2016) 128-140.
- 23 [21] X. Ma, C. Huang, J. Moering, M. Ruppert, H.W. Hoepfel, M. Goeken, J. Narayan, Y. Zhu,
24 Mechanical properties of copper/bronze laminates: Role of interfaces, *Acta Mater.* 116 (2016)
25 43-52.

- 1 [22] M. Zha, H.-M. Zhang, Z.-Y. Yu, X.-H. Zhang, X.-T. Meng, H.-Y. Wang, Q.-C. Jiang,
2 Bimodal microstructure A feasible strategy for high-strength and ductile metallic materials, J.
3 Mater. Sci. Technol. 34(2) (2018) 257-264.
- 4 [23] J. Zhang, S. Hao, D. Jiang, Y. Huan, L. Cui, Y. Liu, H. Yang, Y. Ren, In situ synchrotron
5 high-energy X-ray diffraction study of microscopic deformation behavior of a hard-soft dual
6 phase composite containing phase transforming matrix, Acta Mater. 130 (2017) 297-309.
- 7 [24] H. Wu, G. Fan, M. Huang, L. Geng, X. Cui, R. Chen, G. Peng, Fracture behavior and strain
8 evolution of laminated composites, Compos. Struct. 163 (2017) 123-128.
- 9 [25] L.J. Huang, L. Geng, H.X. Peng, Microstructurally inhomogeneous composites: Is a
10 homogeneous reinforcement distribution optimal?, Prog. Mater Sci. 71 (2015) 93-168.
- 11 [26] E.I. Salama, A. Abbas, A.M.K. Esawi, Preparation and properties of dual-matrix carbon
12 nanotube-reinforced aluminum composites, Composites Part A 99 (2017) 84-93.
- 13 [27] K. Ma, Z.Y. Liu, B.S. Liu, B.L. Xiao, Z.Y. Ma, Improving ductility of bimodal carbon
14 nanotube/2009Al composites by optimizing coarse grain microstructure via hot extrusion,
15 Composites Part A 140 (2021) 106198.
- 16 [28] M. Huang, C. Xu, G. Fan, E. Maawad, W. Gan, L. Geng, F. Lin, G. Tang, H. Wu, Y. Du, D.
17 Li, K. Miao, T. Zhang, X. Yang, Y. Xia, G. Cao, H. Kang, T. Wang, T. Xiao, H. Xie, Role of
18 layered structure in ductility improvement of layered Ti-Al metal composite, Acta Mater. 153
19 (2018) 235-249.
- 20 [29] Z. Lee, V. Radmilovic, B. Ahn, E.J. Lavernia, S.R. Nutt, Tensile Deformation and Fracture
21 Mechanism of Bulk Bimodal Ultrafine-Grained Al-Mg Alloy, Metall. Mater. Trans. A 41(4)
22 (2010) 795-801.
- 23 [30] J.S. Hayes, R. Keyte, P.B. Prangnell, Effect of grain size on tensile behaviour of a
24 submicron grained Al-3 wt-%Mg alloy produced by severe deformation, Mater. Sci. Technol.
25 16(11-12) (2000) 1259-1263.

- 1 [31] J. Inoue, S. Nambu, Y. Ishimoto, T. Koseki, Fracture elongation of brittle/ductile
2 multilayered steel composites with a strong interface, *Scripta Mater.* 59(10) (2008) 1055-1058.
- 3 [32] C.X. Huang, Y.F. Wang, X.L. Ma, S. Yin, H.W. Hoppel, M. Goken, X.L. Wu, H.J. Gao,
4 Y.T. Zhu, Interface affected zone for optimal strength and ductility in heterogeneous laminate,
5 *Mater. Today* 21(7) (2018) 713-719.
- 6 [33] C. Shao, S. Zhao, X. Wang, Y. Zhu, Z. Zhang, R.O. Ritchie, Architecture of high-strength
7 aluminum–matrix composites processed by a novel microcasting technique, *NPG Asia*
8 *Materials* 11(1) (2019) 69.
- 9 [34] X. Fu, Z. Tan, X. Min, Z. Li, Z. Yue, G. Fan, D.-B. Xiong, Z. Li, Trimodal grain structure
10 enables high-strength CNT/Al-Cu-Mg composites higher ductility by powder assembly &
11 alloying, *Materials Research Letters* 9(1) (2021) 50-57.
- 12 [35] Y.N. Zan, Y.T. Zhou, Z.Y. Liu, G.N. Ma, D. Wang, Q.Z. Wang, W.G. Wang, B.L. Xiao,
13 Z.Y. Ma, Enhancing strength and ductility synergy through heterogeneous structure design in
14 nanoscale Al₂O₃ particulate reinforced Al composites, *Mater. Des.* 166 (2019) 107629.
- 15 [36] K. Lu, Making strong nanomaterials ductile with gradients, *Science* 345(6203) (2014)
16 1455-1456.
- 17 [37] H.P. Klug, L.E.C. Alexander, *X-Ray Diffraction Procedures For Polycrystalline And*
18 *Amorphous Materials*, 1954.
- 19 [38] J.S. Benjamin, T.E. Volin, MECHANISM OF MECHANICAL ALLOYING, *Metall*
20 *Trans* 5(8) (1974) 1929-1934.
- 21 [39] K. Ma, Z.Y. Liu, S. Bi, X.X. Zhang, B.L. Xiao, Z.Y. Ma, Microstructure evolution and hot
22 deformation behavior of carbon nanotube reinforced 2009Al composite with bimodal grain
23 structure, *Journal of Materials Science & Technology* 70 (2021) 73-82.
- 24 [40] Z.Y. Liu, K. Ma, G.H. Fan, K. Zhao, J.F. Zhang, B.L. Xiao, Z.Y. Ma, Enhancement of the
25 strength-ductility relationship for carbon nanotube/Al–Cu–Mg nanocomposites by material

- 1 parameter optimisation, *Carbon* 157 (2020) 602-613.
- 2 [41] Y. Zhao, T. Topping, Y. Li, E.J. Lavernia, Strength and ductility of bi-modal Cu, *Adv. Eng.*
3 *Mater.* 13(9) (2011) 865-871.
- 4 [42] L. Tian, A. Russell, T. Riedemann, S. Mueller, I. Anderson, A deformation-processed
5 Al-matrix/Ca-nanofilamentary composite with low density, high strength, and high
6 conductivity, *Mater. Sci. Eng., A* 690 (2017) 348-354.
- 7 [43] Y. Shi, M. Li, D. Guo, T. Ma, Z. Zhang, G. Zhang, X. Zhang, Tailoring grain size
8 distribution for optimizing strength and ductility of multi-modal Zr, *Mater. Lett.* 108 (2013)
9 228-230.
- 10 [44] B. Chen, J. Shen, X. Ye, L. Jia, S. Li, J. Umeda, M. Takahashi, K. Kondoh, Length effect
11 of carbon nanotubes on the strengthening mechanisms in metal matrix composites, *Acta Mater.*
12 140 (2017) 317-325.
- 13 [45] G. Fan, Y. Jiang, Z. Tan, Q. Guo, D.-b. Xiong, Y. Su, R. Lin, L. Hu, Z. Li, D. Zhang,
14 Enhanced interfacial bonding and mechanical properties in CNT/Al composites fabricated by
15 flake powder metallurgy, *Carbon* 130 (2018) 333-339.
- 16 [46] S. Dong, J. Zhou, D. Hui, Y. Wang, S. Zhang, Size dependent strengthening mechanisms
17 in carbon nanotube reinforced metal matrix composites, *Composites Part A* 68 (2015) 356-364.
- 18 [47] Y.M. Wang, M.W. Chen, F.H. Zhou, E. Ma, High tensile ductility in a nanostructured
19 metal, *Nature* 419(6910) (2002) 912-915.
- 20 [48] D. Witkin, Z. Lee, R. Rodriguez, S. Nutt, E. Lavernia, Al-Mg alloy engineered with
21 bimodal grain size for high strength and increased ductility, *Scripta Mater.* 49(4) (2003)
22 297-302.
- 23 [49] A.M.K. Esawi, N.T. Aboulkhair, Bi-modally structured pure aluminum for enhanced
24 strength and ductility, *Mater. Des.* 83 (2015) 493-498.
- 25 [50] L. Zhu, S. Shi, K. Lu, J. Lu, A statistical model for predicting the mechanical properties of

1 nanostructured metals with bimodal grain size distribution, *Acta Mater.* 60(16) (2012)
2 5762-5772.

3 [51] Y.F. Wang, C.X. Huang, Q. He, F.J. Guo, M.S. Wang, L.Y. Song, Y.T. Zhu,
4 Heterostructure induced dispersive shear bands in heterostructured Cu, *Scripta Mater.* 170
5 (2019) 76-80.

6 [52] U. Krupp, H. Knobbe, H.-J. Christ, P. Koster, C.-P. Fritzen, The significance of
7 microstructural barriers during fatigue of a duplex steel in the high- and very-high-cycle-fatigue
8 (HCF/VHCF) regime, *Int. J. Fatigue* 32(6) (2010) 914-920.

9 [53] Y. Guo, T.B. Britton, A.J. Wilkinson, Slip band–grain boundary interactions in
10 commercial-purity titanium, *Acta Mater.* 76 (2014) 1-12.

11 [54] T.L. Anderson, *Fracture mechanics: fundamentals and applications*, CRC press 2017.

12 [55] R. Bucci, Selecting aluminum alloys to resist failure by fracture mechanisms, *Engineering*
13 *Fracture Mechanics* 12(3) (1979) 407-441.

14

1

Table 1 Statistics of the DZs in various heterogeneous CNT/2009Al composites

| Samples | Numerical statistics of the DZ | | |
|---------------|--------------------------------|--------------------------|-------------|
| | Width (μm) | Length (μm) | Content (%) |
| 3% CNT-0 h DZ | 2.62 | | 26.4 |
| 3% CNT-3 h DZ | 2.56 | >100 | 25.3 |
| 3% CNT-4 h DZ | 6.62 | | 27.1 |
| 3% CNT-5 h DZ | 10.45 | | 26.4 |

2

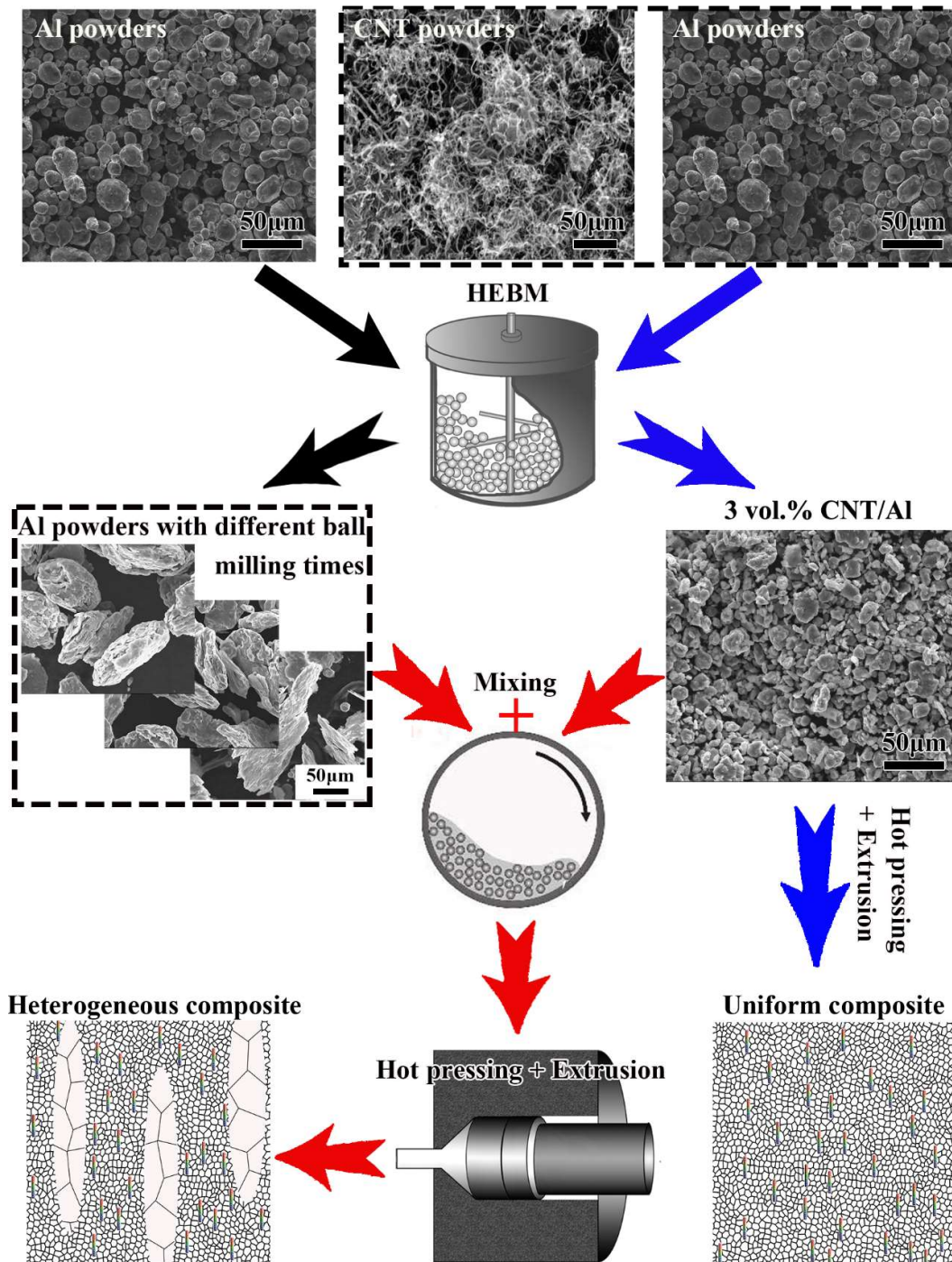
3

Table 2 Tensile properties of 2009Al alloy and CNT/2009Al composite

| Sample | Structure | YS _I (MPa) | YS _{II} (MPa) | UTS (MPa) | EI (%) |
|----------------------------------|---------------|-----------------------|------------------------|-------------|---------------|
| 2009Al-0 h | Uniform, DZ | 305 \pm 2 | - | 427 \pm 3 | 12 \pm 1.0 |
| 2009Al-4 h | Uniform, DZ | 515 \pm 4 | - | 536 \pm 5 | 11 \pm 1.0 |
| uniform 2.25 vol.% CNT/2009Al | Uniform, BZ | 671 \pm 5 | - | 707 \pm 5 | 2.5 \pm 0.2 |
| uniform 3 vol.% CNT/2009Al | Uniform, BZ | 672 \pm 5 | - | 715 \pm 6 | 2.3 \pm 0.2 |
| 3% CNT-0 h DZ | Heterogeneous | 574 \pm 5 | 625 \pm 5 | 680 \pm 8 | 3.8 \pm 0.5 |
| 3% CNT-3 h DZ | Heterogeneous | 601 \pm 6 | 633 \pm 4 | 689 \pm 7 | 3.6 \pm 0.5 |
| 3% CNT-4 h DZ | Heterogeneous | 620 \pm 7 | 655 \pm 6 | 720 \pm 6 | 4.7 \pm 0.5 |
| 3% CNT-5 h DZ | Heterogeneous | 623 \pm 5 | 658 \pm 5 | 708 \pm 9 | 4.0 \pm 0.5 |

4

5

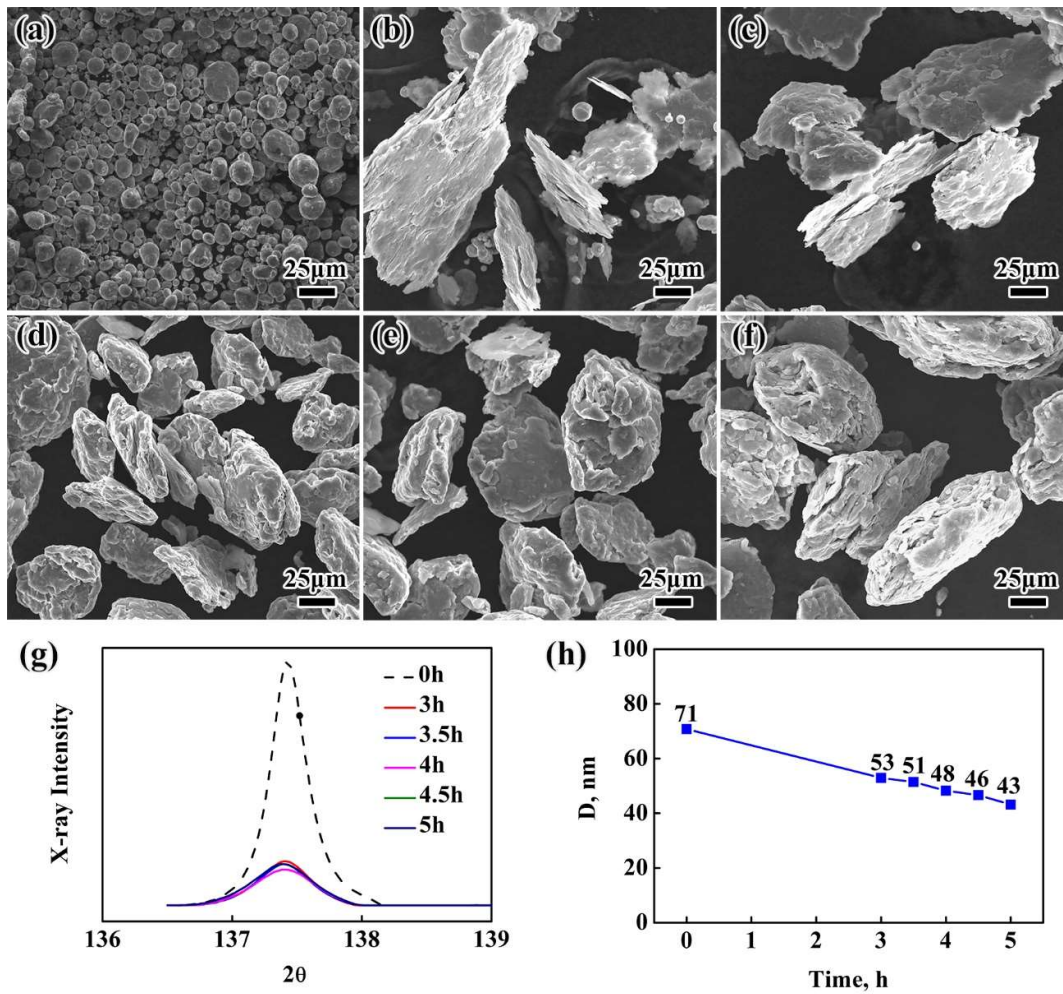


1

2

3

Fig. 1 Schematic of fabrication process of CNT/2009Al composites with heterogeneous structure.

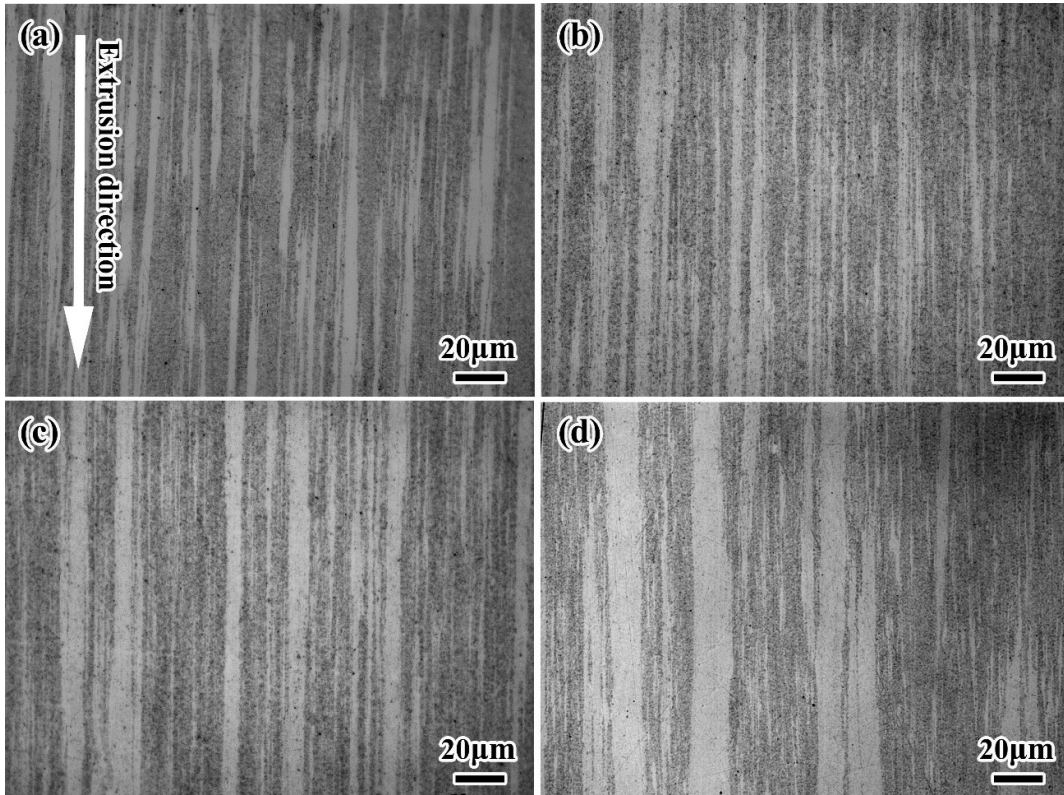


1

2 **Fig. 2** Morphology of 2009Al powders milled for different times: (a) 0 h, (b) 3 h, (c) 3.5 h, (d)

3 4 h, (e) 4.5 h, (f) 5 h; (g) XRD diffraction patterns of 2009Al powders milled for different

4 times, (h) subgrain size (D) evolution with milling time.

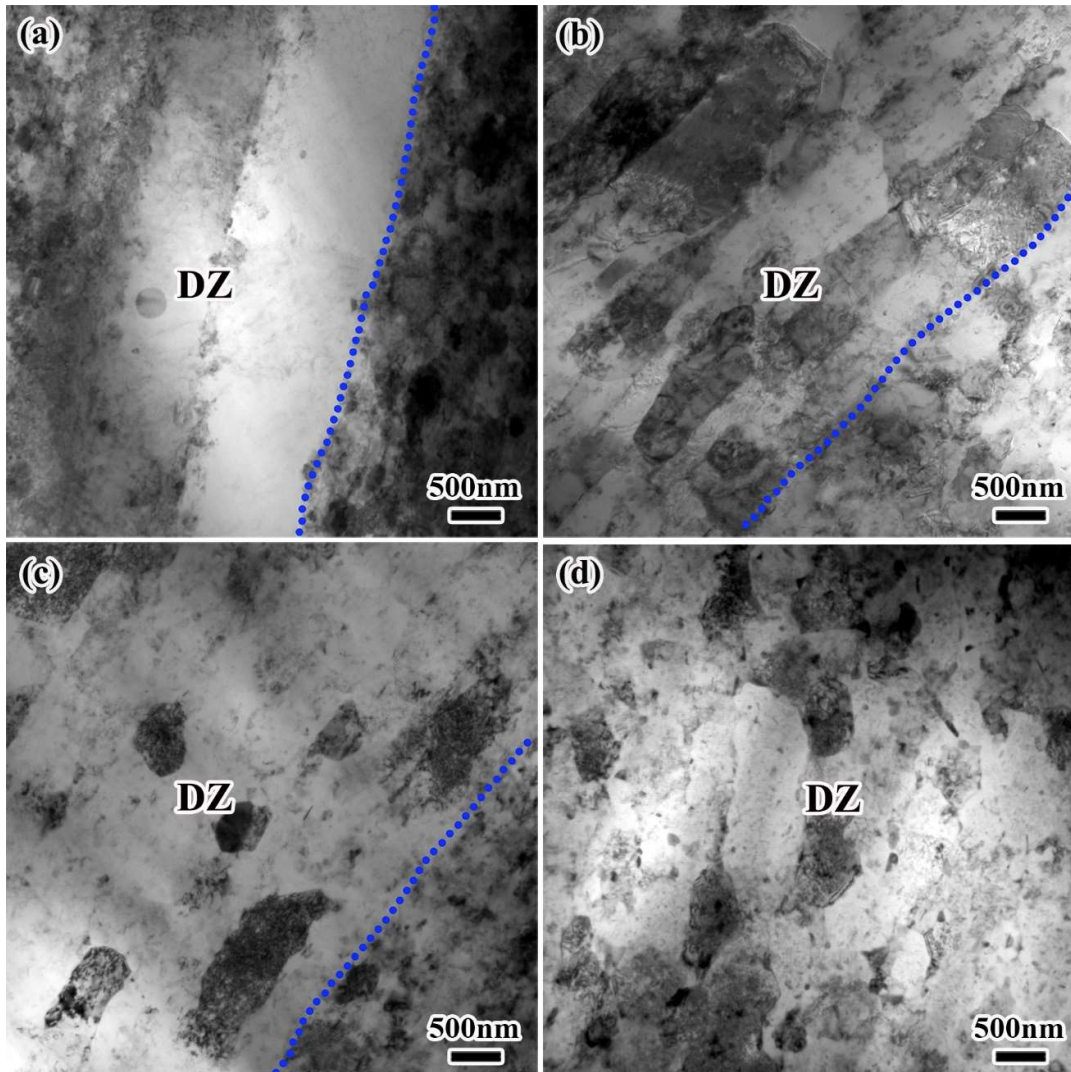


1

2 **Fig. 3** OM images of different heterogeneous CNT/2009Al composites: (a) 3% CNT-0 h DZ,

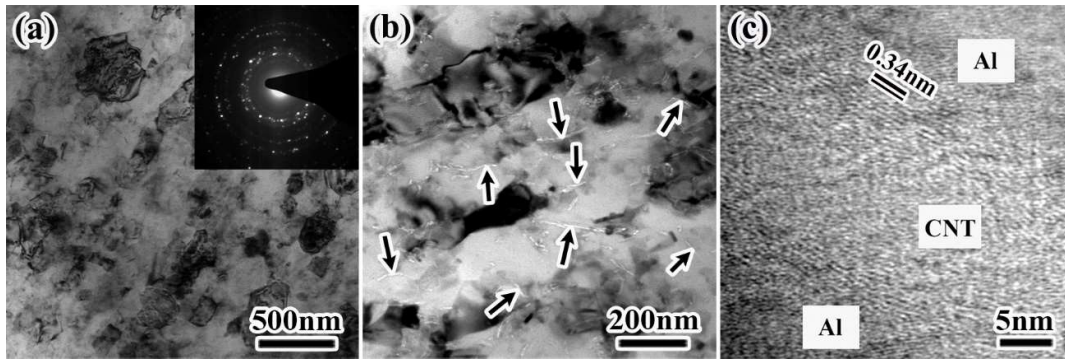
3

(b) 3% CNT-3 h DZ, (c) 3% CNT-4 h DZ, (d) 3% CNT-5 h DZ.

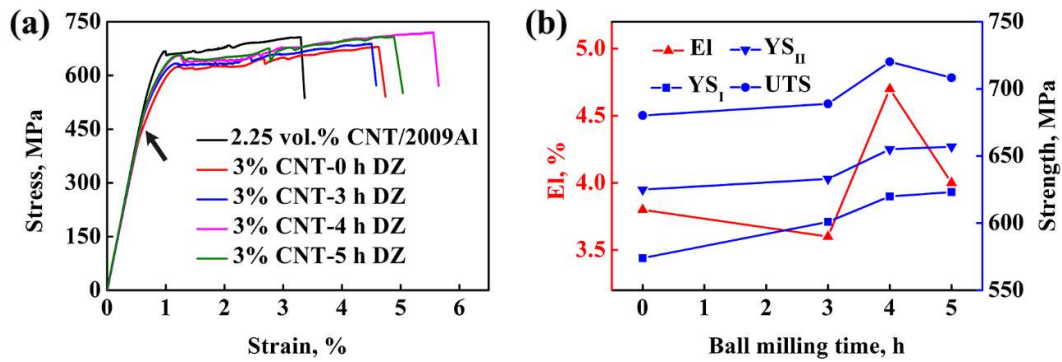


1
2
3
4
5

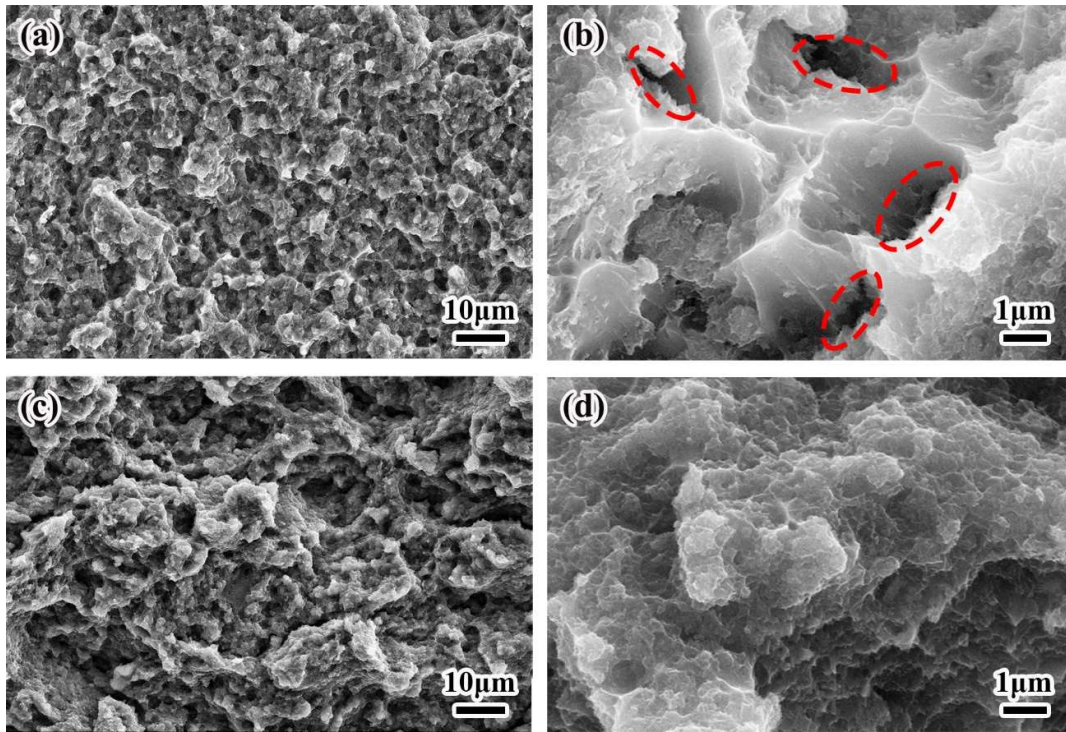
Fig. 4 TEM images of DZs in different heterogeneous CNT/2009Al composites: (a) 3% CNT-0 h DZ, (b) 3% CNT-3 h DZ, (c) 3% CNT-4 h DZ, (d) 3% CNT-5 h DZ (Blue lines are the boundaries between the DZs and the BZs).



1
2 **Fig. 5** TEM images of BZs of 3% CNT-4h DZ: (a) grain morphology, (b) CNT distribution,
3 and (c) CNT-Al interface.



5
6 **Fig. 6** Mechanical properties of uniform 2.25vol.% CNT/2009Al and different heterogeneous
7 CNT/2009Al composites: (a) engineering strain-stress curves and (b) property values of
8 heterogeneous composites vs. ball milling time of additional 2009Al powders.

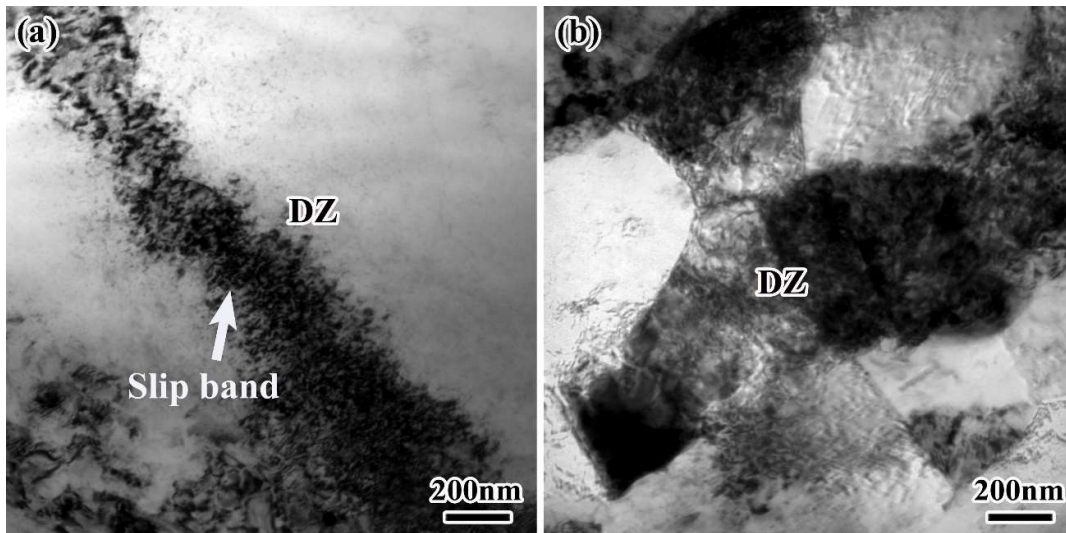


1

2 **Fig. 7** Fractographs of two typical heterogeneous composites: (a)(b) 3% CNT-0 h DZ, (c)(d) 3%

3

CNT-4 h DZ.

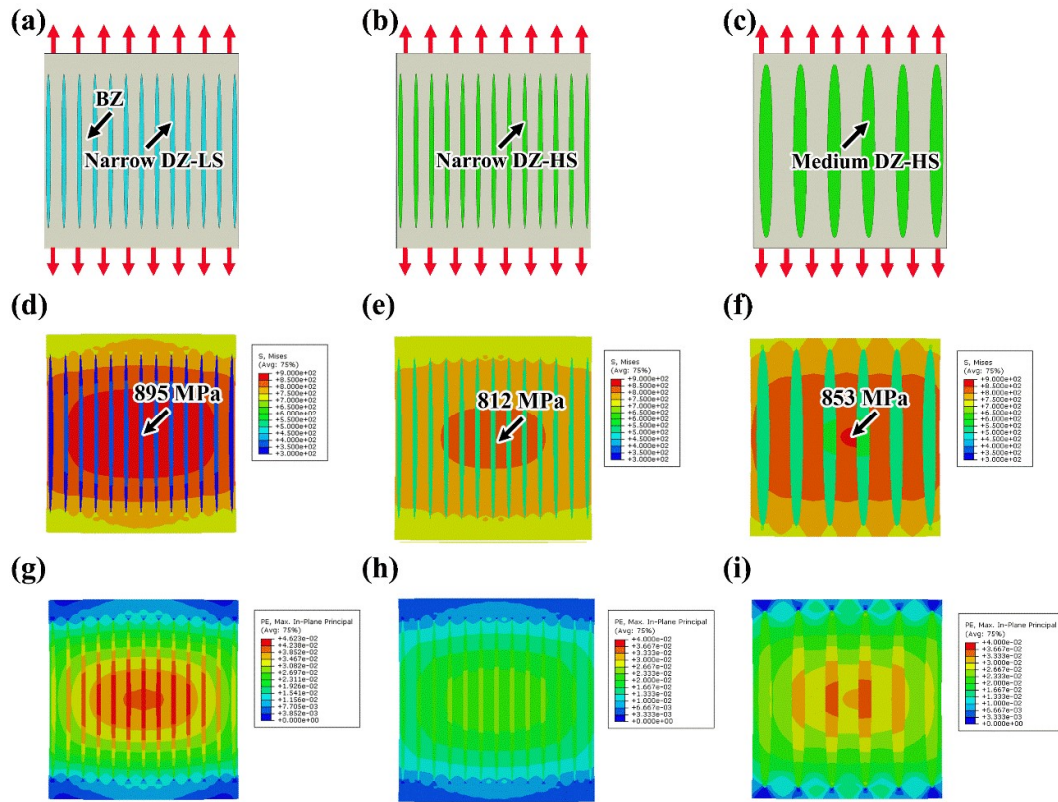


4

5 **Fig. 8** TEM images of DZs after 2% plastic strain for two typical heterogeneous composites:

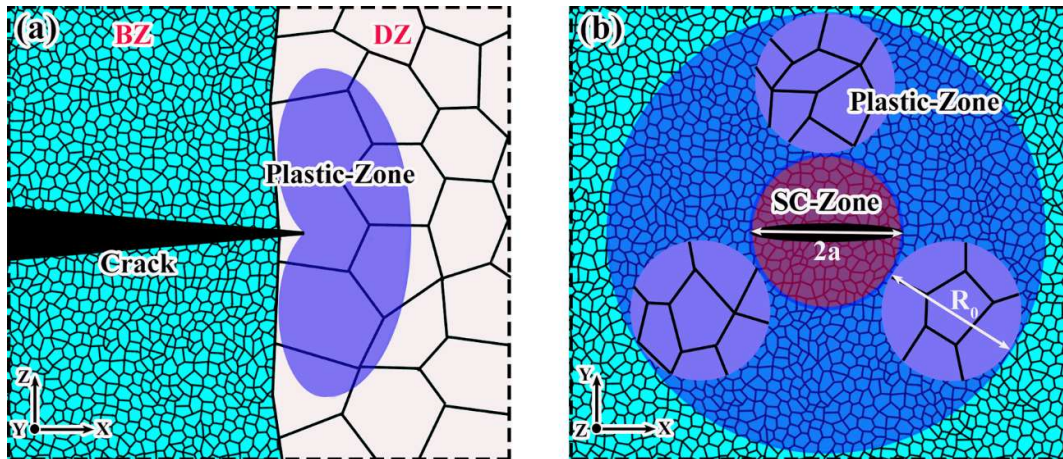
6

(a) 3% CNT-0 h DZ and (b) 3% CNT-4 h DZ.



1
2
3
4

Fig. 9 2-D FEM simulation results: (a)(b)(c) models of heterogeneous materials containing different DZs, (d)(e)(f) stress distribution map, (g)(h)(i) strain distribution map.



5
6
7
8

Fig. 10 Schematic of toughening mechanism in heterogeneous materials: (a) stress concentration at the micro-crack tip induced plastic zone in DZ and (b) crack blunting by joint action of multiple neighboring DZs.